Original Article

Intra-frame Motion Compensation in Multi-frame Brain PET Imaging

Hassan Mohy-ud-Din[1, 2, *], Nicolas A. Karakatsanis[3], William Willis[2], Abdel K. Tahari[2], Dean F. Wong[2], and Arman Rahmim[1, 2]

1- Department of Electrical and Computer Engineering, Johns Hopkins University, MD, USA.
2- Department of Radiology and Radiological Sciences, Johns Hopkins School of Medicine, MD, USA.
3- Division of Nuclear Medicine, University of Geneva, Geneva, Switzerland.

Received: 1 March 2015
Accepted: 22 April 2015

A B S T R A C T

Purpose- Inter-frame and intra-frame motion can adversely impact the performance of dynamic brain PET imaging. Only correcting the former can still result in degraded qualitative and quantitative performance. Meanwhile, patient motion introduces mismatches between transmission and emission data which may lead to incorrect attenuation and scatter compensation in the reconstruction process. As a result, the reconstructed dynamic images may carry erroneous estimates of radioactivity distribution. We seek a solution to this problem.

Methods- We investigated the use of iterative deconvolution coupled with a proposed use of time-weighted averaging of motion-transformed transmission images to correct the transmission-emission mismatch artifacts in dynamic brain PET images. We performed simulations using real-patient motion profile acquired by the infrared Polaris Vicra motion tracking device which estimates 3-D motion transformations during PET acquisition. This was followed by frame-based motion correction employing three different transmission-emission alignment strategies: transmission image transformed by (1) mean motion transformation, (2) median motion transformation, and (3) the proposed time-weighted average of motion-transformed transmission images.

Results- The results demonstrate that the proposed approach of using time-weighted averaging of motion transformed transmission images outperforms conventional methods by substantially reducing the transmission-emission mismatch artifacts in the reconstructed images. Coupled with an alignment of the reconstructed frames for inter-frame motion correction and a subsequent iterative deconvolution approach for intra-frame motion correction, the resulting motion compensated images showed superior quality, considerable reduction in error norm and enhanced noise-bias performance compared to conventional methods of transmission-emission mismatch compensation. The performance was consistent across different levels of intra-frame motion, and the algorithm was amenable to different framing schemes.

Conclusion- In frame-based motion correction of dynamic PET images, it is feasible to achieve intra-frame motion compensation using time-weighted averaging of motion transformed transmission images coupled with a post-reconstruction iterative deconvolution procedure to compensate for intra-frame motion.

Keywords:
Dynamic PET imaging,
Transmission/ Emission mismatch artifacts,
Inter-frame and Intra-frame motion,
Motion compensation.

1. Introduction

Positron Emission Tomography is a powerful imaging technique enabling *in vivo* measurements of neurochemistry and neuropathology [1, 2]. High-resolution brain PET imaging allows image acquisitions with a spatial resolution of 2–5 mm FWHM range [3]. Despite enhanced spatial resolution, PET images can be severely degraded by patient motion, thereby undermining the high-resolution capability of a

**** Corresponding Author:***
Hassan Mohy-ud-Din, PhD
Department of Diagnostic Radioloy, Yale School of Medicine, Yale University.
Tel: (+1) 4433017004
E-mail:hassan.mohy-ud-din@yale.edu

given scanner.

Dynamic brain PET imaging sessions (e.g. for applications such as neuroreceptor mapping and quantification) are typically very long (~60–120 min), making it unreasonable to assume that even very cooperative patients remain still for the entire acquisition duration [4]. There is a greater likelihood of motion in patients who have neurological or psychological disorders resulting in involuntary motion e.g. restless leg syndrome and epilepsy [5, 6], or Tourette's syndrome [7]. In addition, voluntary head movements due to coughing, leg crossing, etc. are commonly observed in PET scans [8]. If not accounted for, they can result in significant motion artifacts in the reconstructed images.

Motion artifacts degrade the qualitative and quantitative analysis of PET data in the following ways: (1) Patient motion introduces transmission-emission mismatches between transmission and emission acquired data leading to incorrect attenuation and scatter correction in the reconstruction process. As a result, the reconstructed dynamic images may carry erroneous estimates of radioactivity distribution [9, 10]. (2) Patient motion can contaminate the time activity curves (TACs) at a voxel or ROI level resulting in inaccurate estimates of kinetic parameters [11]. (3) It can also cause a loss of contrast due to motion-blurring artifacts leading to a poor discernibility of small structures such as lesions [12] or small brain structures of neurochemical interests such as the ventral striatum.

A solution to motion compensation in dynamic PET imaging has been the method of Multiple Acquisition Frames (MAF) [13]. MAF re-frames the dataset in accordance with motion thresholds, followed by inter-frame motion correction. There are three drawbacks to this: (1) the introduction of a low motion threshold may result in acquisition of low-statistic frames, thereby degrading image quality and increasing the number of frames to be reconstructed [14]. (2) By contrast, the use of a high motion threshold will result in considerable intra-frame motion. (3) Finally and importantly, in common practice, dynamic PET studies are reconstructed using a tracer-specific framing sequence and this consistency is much preferred over a motion-dependent framing sequence which may be different even for the same subject scanned multiple times.

Another solution is to correct the individual lines of response (LORs) for motion [6, 15]. This approach requires access to and processing of the original list-mode data. More importantly, it has been shown that mere motion-compensation of LORs can lead to artifacts, and must be accompanied by modifying probabilities of detection due to motion [16-20], posing additional algorithmic and computational complexity to the problem. As a result of these, there has been a preference in routine practice by the dynamic brain PET imaging community to focus on inter-frame motion compensation only [21, 22].

Such inter-frame motion compensation has been achieved by (a) algorithms (e.g. automated image registration (AIR) software) that re-align PET frames to a reference frame [10, 12, 22, 23]; or (b) algorithms that employ motion information acquired from optical tracking apparatus [6, 13, 24, 25]. In any case, we note that these approaches neglect the intra-frame motion compensation, which are studied by the present work.

We focus on the use of external motion tracking (e.g. Polaris Vicra tracking as commonly used in a number of brain PET imaging centers). In the context of single-frame static brain PET imaging, an approach investigated by Faber *et al*. [24] was to employ Richardson-Lucy (R-L) iterative deconvolution on motion-contaminated PET images to estimate the original non-corrupted image. We extend this work in three ways: (1) by focusing on the multi-frame PET imaging context, wherein inter-frame and (post-reconstruction) intra-frame motion compensation are both performed. (2) An issue not quantified by Faber *et al*. [24] that we carefully study is the occurrence of attenuation artifacts that arise from transmission-emission mismatches. We study this issue elaborately and show that these mismatch artifacts can become significant with increasing levels of intra-frame motion. (3) To alleviate this issue, this work proposes an employment of time-weighted averaging of motion transformed transmission images for more accurate attenuation correction in image reconstruction [26, 27].

2. Methodology

2.1. Transmission-Emission Alignment Strategies

Subject motion results in spatial misalignment between transmission and emission scans, leading to inaccurate attenuation and scatter correction in the reconstruction process. A common solution

to this is to align the transmission image to some 'average' position of the emission object within the particular frame of interest. An example of this 'average' position includes either the mean or the median motion transform (items 1 and 2 below). However, we have observed in the present work that in the case of considerable intra-frame motion, these approaches are sub-optimal, and that an alternative approach is considerably more rewarding. There is a difference between mappings by an average motion transform, versus averaging of images mapped by different motion transforms. We propose the latter which turns out to be particularly advantageous in producing motion compensated images with higher qualitative and quantitative accuracy compared to conventional approaches. Thus, we investigate three transmission-emission alignment strategies to tackle mismatch artifacts in reconstructed images:

Conventional Approaches

1. Transmission Image Transformed by Median Motion Transformation: For each dynamic frame J, the transmission image is transformed by the middle motion transformation that occurs in the Jth frame, and is then forward projected to generate attenuation correction factors (ACFs). However, the more common conventional approach is as follows.

2. Transmission Image Transformed by Mean Motion Transformation: For each dynamic frame *J*, the transmission image is transformed by the mean motion transformation $\overline{M^J}$, and is then forward projected to generate ACFs [11].

Proposed Approach

3. Time-weighted Average of Motion Transformed Transmission Images: For each dynamic frame *J*, the transmission image is first transformed by each of the N_J significant motion transformations to generate N_J copies of motion transformed transmission images. This is followed by computing a time-weighted average of the motion transformed transmission images, which is then forward projected to generate ACFs.

To see this better, we note that for an object f_{M_i} at a time/ position with motion transformation M_i (i =1…N), the expected value of projected data Y (prior to adding accidental coincidences), is given by:

$$Y = \sum_{i=1}^{N} w_i A_{M_i} P f_{M_i} \quad (1)$$

where T is the frame duration, ΔT_i is the duration of the i^{th} motion state in the concerned frame, $w_i = \Delta T_i / T$ is the time weight for each motion transformation and $\sum_i w_i = 1$, P denotes the projection matrix including everything (e.g. image-space blurring, geometric projection and normalization) except for the effect of attenuation which is modified with each motion because of the fact that the transmission image is itself also moving, and is given by A_{M_i}. (note that technically, for better accuracy, the effect of radioactive decay can/ should also be incorporated in the weights w_i; see discussion section). For a given frame with mean motion $\overline{M}$, conventional methods assume the following approximation:

$$Y = \sum_{i=1}^{N} w_i A_{\overline{M}} P f_{M_i} = A_{\overline{M}} P \sum_{i=1}^{N} w_i f_{M_i} \quad (2)$$

thus arriving at a single sinogram $A_{\overline{M}}$ for attenuation correction of the motion-degraded frame. By contrast, the proposed method effectively assumes the following:

$$Y = \left(\sum_{i=1}^{N} w_i A_{M_i} \right) P \left(\sum_{i=1}^{N} w_i f_{M_i} \right) = \overline{A_M} \, P \sum_{i=1}^{N} w_i f_{M_i} \quad (3)$$

where $\overline{A_M}$ denotes the overall attenuation sinogram obtained by time-weighted averaging. A fast method to approximate $\overline{A_M}$ is to actually perform time-weighted averaging of the transmission images, followed by forward-projection to obtain mean attenuation sinogram, as opposed to the computationally intense approach of performing individual forward-projections of motion-transformed transmission images, followed by averaging. In fact, we observed both approaches to produce images of very comparable quantitative performance, and hence pursued the computationally faster approach in what follows.

2.2. Inter-frame and Intra-frame Motion Correction

Following transmission-emission alignment using the above-mentioned methods and reconstruction of

the frames, we performed an inter-frame alignment of the emission images. Specifically, each independently reconstructed image at a given frame *J*, with a time-weighted mean motion $\overline{M^J}$, was transformed by $(\overline{M^J})^{-1}$ to provide a correctly registered set of dynamic images.

To compensate for intra-frame motion, we first computed the net residual motion in each independently reconstructed frame by 'removing' the mean motion transformation from the motion transformations M_i^J at each significant motion state *i* in each frame *J*; i.e. $M_i^{J,residual} = (\overline{M^J})^{-1}.M_i^J$. This was followed by iteratively removing the residual motion from each reconstructed image via Richardson-Lucy deconvolution [28, 29]:

$$\lambda_J^{n+1} = \lambda_J^n \sum_{i=1}^{N_J} w_i^J \left(M_i^{J,residual}\right)^{-1} \left\{ \frac{Q_J}{\sum_{i=1}^{N_J} w_i^J M_i^{J,residual} \{\lambda_J^n\}} \right\} \quad (4)$$

where Q_J is the inter-frame motion corrected emission image (i.e. $Q_J = (\overline{M^J})^{-1}\{I_J^{recon}\}$ I_J^{recon} is the reconstructed emission image for frame J), N_J is the number of significant motion transformations ($i = 1,..., N_J$), w_i^J denotes the corresponding time weights for frame J, and λ_J^n is the intra-frame motion corrected emission image at iteration. We also performed inter-iteration smoothing with a Gaussian filter (FWHM 2 mm) to control noise propagation in iterative deconvolution.

3. Experimental Design

3.1. Tomograph

PET data was acquired on the second generation High Resolution Research Tomograph (HRRT) [30]. The detector heads in the octagonal design consist of a double 10 mm layer of LSO/LYSO for a total of 119, 808 detector crystals (crystal size 2.1 x 2.1 x 10 mm^3). The total number of possible LORs is 4.486 x 10^9. The dimensions of the reconstructed image are 256×256×207 and the voxel volume is 1.219×1.219×1.219 mm^3. The images were reconstructed using the Ordered Subsets Expected Maximization (OSEM) algorithm (10 iterations, 16 subsets).

3.2. Phantom

We used a mathematical brain phantom [31] to conduct simulation studies based on a real patient motion profile. The phantom is constructed using subdivision surfaces enabling efficient modeling of arbitrary topological structures like brain, skull, muscle tissue, and vasculature [31]. The details on surface modeling are contained in [31] and the references therein. Figure 1 shows the transaxial, coronal and sagittal slices of the phantom. The activity numbers in the phantom were derived from a human FDG PET study.

3.3. Polaris Motion Tracking and Calibration

We used the Polaris Vicra [8, 32] to track typical head movements in a human subject. The Polaris Vicra is a high-resolution (< 0.1mm) infrared (IR) optoelectronic system that uses 4 IR retro-reflective spheres in a known geometry. It is fixed to the head via an elastic swimming cap. The 4 spheres face the Polaris inside the gantry which in turn acquires motion-transformations at 30 ms time resolution. Polaris motion tracking is insensitive to lighting conditions, uses significantly less disk space for data storage (in comparison to optical image sequences) and is commercially available and economical [14].

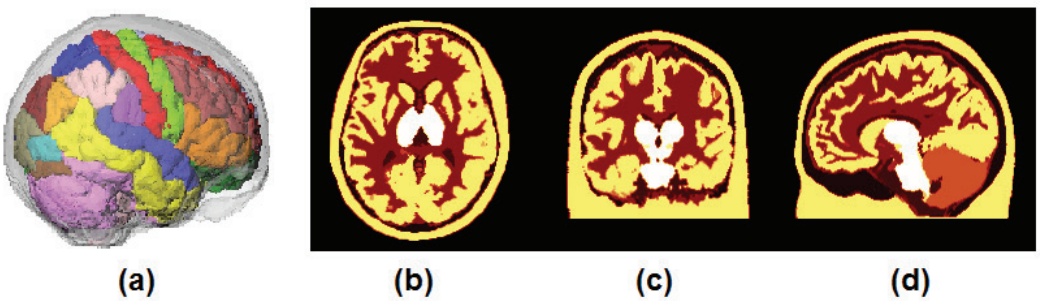

Figure 1. (a) Mathematical Brain Phantom, (b) – (d) Transaxial, Coronal, and Saggital slices of the phantom.

Polaris-to-Tomograph transformation, $[P2T]_{4x4}$, was computed via a series of calibration experiments performed simultaneously with Polaris tracking and transmission scan measurements [19, 31]. The Polaris tool was placed in a static position in the scanner and the coordinates of its center along with its orientation (quaternion and translation vectors) were determined. Given the knowledge of the relative positions of the 4 spheres, the 3-D positions of the spheres were extracted. During this time, a 10 min transmission scan of the tracking tool was also obtained. From the reconstructed transmission image, the coordinates of the 4 spheres were determined by first isolating the 4 spheres from the clamp-plate and then fitting a 3-D Gaussian to the center of each sphere. This entire process was repeated 10 times to increase the accuracy of the calibration. $[P2T]_{4x4}$ was obtained by employing a least squares fit to the Polaris and tomograph measurements [33]. $[P2T]_{4x4}$ is later applied during the post-reconstruction motion compensation procedure.

The motion file generated by Polaris Vicra consists of motion transformations in the form of a quaternion vector, $[q_0\ q_1\ q_2\ q_3]$, and a translation vector, $[t_x\ t_y\ t_z]$ i.e. 7 numbers. We first averaged the motion transformations accumulated over a series of 1 second intervals to reduce Polaris measurement noise. This gave us motion transformations at each second of time interval. Subsequently, we applied a combination of motion threshold (0.3 – 1 mm) and a time threshold of 15 seconds duration to get significant motion transformations. The motion threshold (of 1 mm) was set to be one-third of the PET system resolution at the center of the field of view [34]. A time threshold of 15 seconds was empirically chosen to eliminate impulsive motion; i.e. movements that last for very short durations.

3.4. Subject Study

A human subject was recruited to be scanned on the HRRT scanner following a clinical (non-research) FDG PET scan. The patient was consented and enrolled under a JHU IRB approved research protocol and monitored for safety by a study physician during participation. No adverse events were observed or reported. The Polaris Vicra and PET acquisition system were synchronized with a master clock using TCL scripts. The tracking tool was fixed to the patient's head via an elastic swimming cap. Before scanning, appropriate measures were taken to minimize relative motion between the tracker and the patient's head and to ensure that the tracker did not slip away during scanning. The patient was injected with 20 mCi of FDG 1.75 hrs prior to scanning.

A transmission scan was performed for the first 6 minutes followed by a 25 minutes emission scan. The patient was asked to remain very still during the transmission scan and the first 5 minutes of the emission scan to acquire a reference image with minimal motion. The patient was then asked to make a number of specific movements and finally to move freely for the rest of the study. The Polaris Vicra generated a motion file from which significant motion-transformations for individual frames were extracted.

3.5. Quantitative Metrics

This section elaborates upon the quantitative metrics used to analyze the motion compensated images. The reference image used in these computations corresponded to the first five minutes of emission scan that contained minimal motion. We preferred it over the original true phantom as the latter does not contain partial volume effects [31].

1. Error Norm: The error norm (units of activity) is a voxel-wise comparison between the reference image, R, and the motion-compensated PET image, I. It is defined as follows:

$$I, R = \sum_{i=1}^{V} \left| I[i] - R[i] \right| \tag{5}$$

2. Mean Displacement: We use the time-weighted mean displacement, $\overline{Disp}$, to quantify motion in a dynamic PET image. For each dynamic frame, $\overline{Disp}$ is calculated with respect to the mean motion transformation in that frame ($\overline{M}$):

$$\overline{Disp} = \frac{1}{V} \sum_{i=1}^{V} \sum_{j=1}^{N} w_j \left\| M^j(i) - \overline{M}(i) \right\| \tag{6}$$

where V is the total number of voxels in the masked image, N is the total number of significant

motion transformations in each frame, w_j is the time-weight for the j^{th} motion transformation, and $M(i)$ denotes the spatial coordinates of voxel i under the motion transformation M.

3. Noise and Bias: We quantitatively analyzed different regions of interest (ROIs): white matter, caudate, putamen, cingulate, thalamus, globus pallidus, frontal-orbital gyrus, and occipitotemporal gyrus. For noise-bias analysis, we computed regional bias, *RB*, and regional normalized standard deviation, *RNSD*, for each ROI:

$$RB^r = \frac{\left|\lambda^r - \mu^r\right|}{\mu^r} \quad (7)$$

$$RNSD^r = \frac{\sqrt{\frac{1}{L^r - 1}\sum_{\beta \in r}\left(\lambda^\beta - \lambda^r\right)^2}}{\lambda^r} \quad (8)$$

where r indexes the ROIs, λ^r denotes mean reconstructed activity of ROI r in the motion compensated image, μ^r denotes mean activity of ROI in the reference image, L^r is the total number of voxels in ROI r and $\beta \in r$ indexes them.

4. Results

4.1 Real Subject Motion Profile

Figure 2 shows motion profile from the subject motion tracking study. The markers show the frame time points for 9 frames (1 x 300 seconds, 8 x 150 seconds). The first 5 minutes frames clearly show minimal motion and, hence, is used as a reference frame for qualitative and quantitative analysis. Figure 3 shows motion-trajectory of a reference point located in the brain for 150 seconds frame duration. The magnitude of intra-frame motion, quantified by, is 5.92 mm.

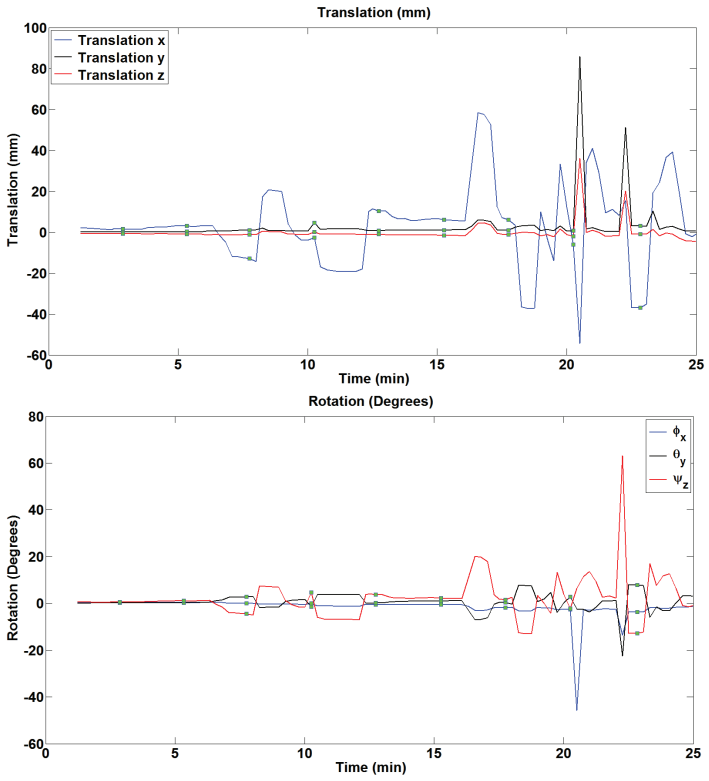

Figure 2. Motion profile acquired during the first 25 minutes of emission scan. Row 1 shows the translation profiles and Row 2 shows the rotation profiles in the three axial directions (**x**, **y**, and **z**). We see a significant translational motion in the **x** axial direction and a significant rotational motion in the **z** axial direction as expected. Green solid markers show the frame time points for the first 9 frames (1 x 300 seconds, 8 x 150 seconds).

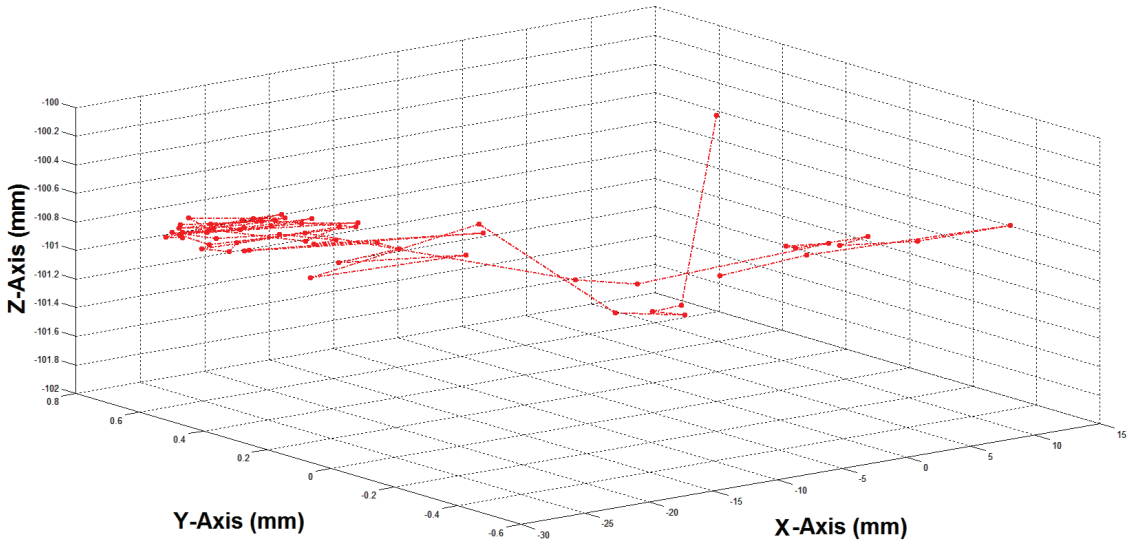

Figure 3. Motion trajectory of a reference point located in the brain during a 150 seconds frame. The origin is at the center of the scanner's FoV. The magnitude of intra-frame motion is 5.92 mm.

4.2. Comparison of Transmission-Emission Alignment Strategies

Qualitative and quantitative comparisons of various motion compensated reconstructed images are depicted in Figures 4 and 5, respectively (Frame 8 with $\overline{Disp}$=4.83 mm and Frame 5 with $\overline{Disp}$=9.08 mm). It is observed that the proposed approach of transmission-emission alignment considerably reduced mismatch artifacts and produced images with superior quality compared to conventional methods. Small regions of interest such as the caudate and putamen were clearly distinguishable, and the functional morphology was preserved for different magnitudes of intra-frame motion. On the contrary, the images from the conventional approach were visibly degraded by transmission-emission mismatch artifacts that degraded the uptake distribution in the caudate and putamen. With increased intra-frame motion (higher $\overline{Disp}$), transmission-emission mismatch becomes increasingly significant, and the motion compensated images from conventional methods degraded severely. The proposed approach showed a substantial improvement even for motion magnitude of ~9 mm. From here on, the results from simulations and subject study will focus only on using the transmission image transformed by the mean (not median) motion $\overline{M^J}$, for each frame J, for conventional approach and using time-weighted average of motion transformed transmission images for the proposed approach.

4.3. Qualitative and Quantitative Analysis of Phantom Simulations

Figure 6 depicts motion compensated images obtained from phantom simulations. We depict results from Frame 5 and Frame 8 with $\overline{Disp}$=4.83 mm and $\overline{Disp}$=9.08 mm respectively. We show motion compensated images with inter-frame motion correction only, as well as additional intra-frame motion correction (with deconvolution iterations 8 and 15 respectively), employing conventional and proposed approaches of transmission-emission alignment.

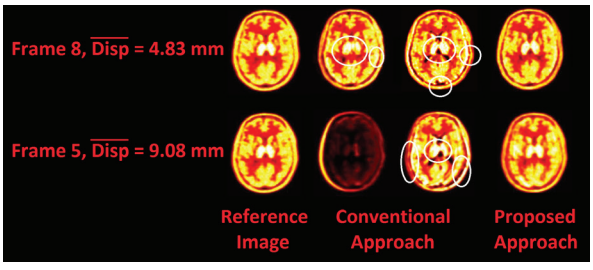

Figure 4. (Rows 1 and 2: L-to-R) (a) reference image, motion compensated image using the transmission image transformed by (b) median and (c) mean motion transformation, and (d) the proposed approach of using time-weighted motion transformed transmission images respectively. White ellipses highlight the artifacts in motion compensated images using conventional approach of transmission-emission alignment.

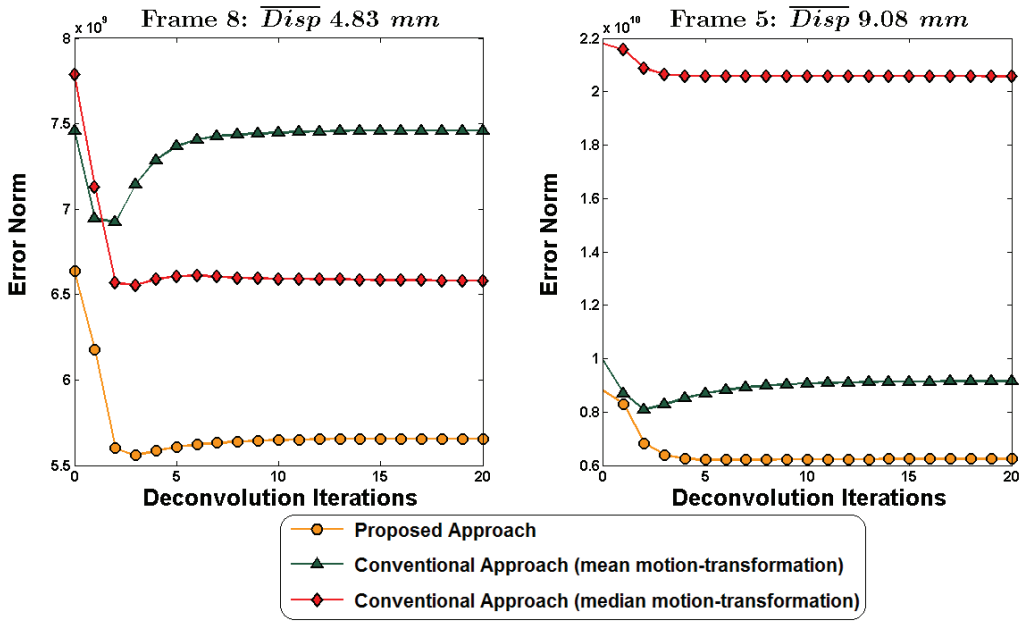

Figure 5. Error norm curves from simulations using different transmission-emission alignment strategies. The proposed approach of using time-weighted motion transformed transmission images clearly outperforms conventional methods for minimizing mismatch artifacts in motion compensated images.

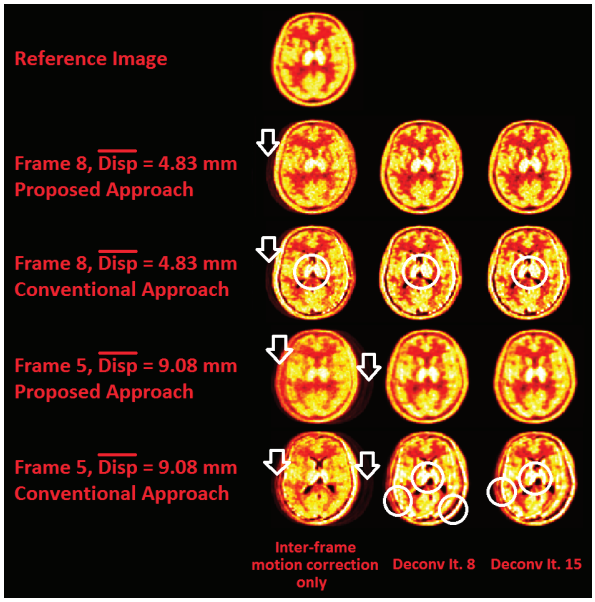

Figure 6. (L-to-R) inter-frame motion compensated images, inter-frame and intra-frame motion compensated images with conventional and proposed approaches of transmission-emission alignment, and deconvolution iterations 8 and 15 respectively. White ellipses highlight artifacts. Proposed approach outperforms conventional methods in producing motion compensated images with superior quality.

Our proposed approach is seen to considerably remove inter-frame and intra-frame motion artifacts. The results are consistent across different levels of intra-frame motion. The conventional approach produced images that are visibly degraded by transmission-emission mismatch artifacts, even with small movements. These artifacts are amplified with increased deconvolution iterations and motion levels. We concluded from this qualitative analysis that the proposed approach produced motion compensated images with superior quality. We now substantiate this assessment through quantitative analysis of motion compensated dynamic images.

Figure 7 shows the error norm curves for the proposed and conventional approaches with varying deconvolution iterations. 0^{th} deconvolution iteration implies inter-frame only motion correction. We omitted frames with negligible intra-frame motion. The proposed approach showed a larger error drop compared to the conventional approach. In fact, for the conventional approach, the error norm increases with deconvolution iterations and intra-frame motion. This is again attributed to transmission-emission mismatch which starts to dominate with a higher intra-frame motion.

Figure 8 shows the Error Norm vs. $\overline{Disp}$ plots for the proposed and conventional approaches with inter-frame and intra-frame motion correction (10 deconvolution iterations). We obtained a proportional relationship between error norm and

$\overline{Disp}$. Conventional approach showed a significant discrepancy with increasing intra-frame motion (quantified by $\overline{Disp}$). Even at higher levels of intra-frame motion (higher $\overline{Disp}$), the proposed approach showed a significantly better error performance compared to the conventional approach.

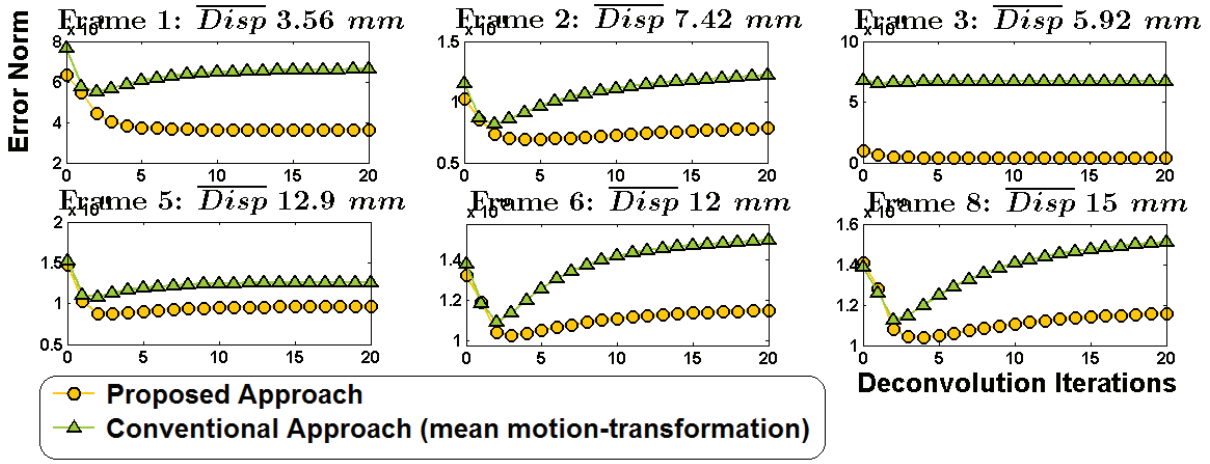

Figure 7. Error norm plot for different frames against deconvolution iterations (10 OSEM iterations, 16 subsets). 0th iteration implies intra-frame only motion correction. Proposed approach outperformed conventional approach exhibiting a larger error drop. Conventional approach showed an increase in error norm because the transmission-emission mismatch starts to dominate with increased deconvolution iterations.

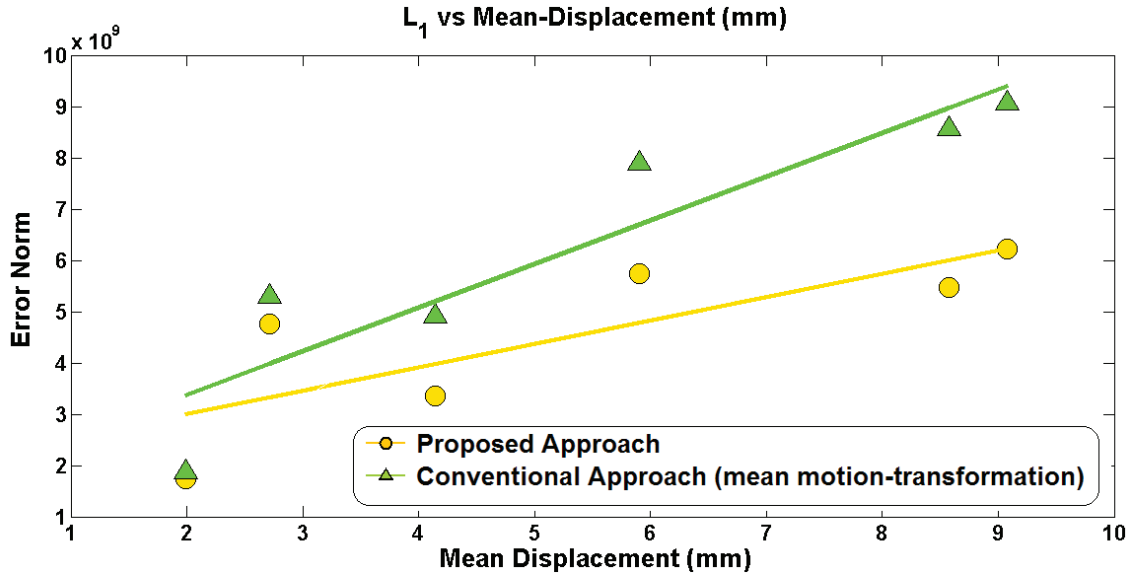

Figure 8. L_1 *vs* $\overline{Disp}$ plot shows increased discrepancy with higher intra-frame motion (higher $\overline{Disp}$). Proposed approach outperforms conventional approach by significantly reducing the transmission-emission mismatch artifacts (as shown by a better error performance).

Figure 9 shows overall noise vs. bias plots for deconvolution iterations 1, 2, 3, 5, 8, 10, 15, and 20 (across 8 ROIs). The proposed approach outperformed the conventional approach in noise vs. bias trade-off at different magnitudes of intra-frame motion. With increasing deconvolution iterations, we saw a greater reduction in bias at a cost of smaller increase in noise levels. For conventional approach, the noise-bias performance worsened with increasing deconvolution iterations, which is attributed to the transmission-emission mismatch artifacts.

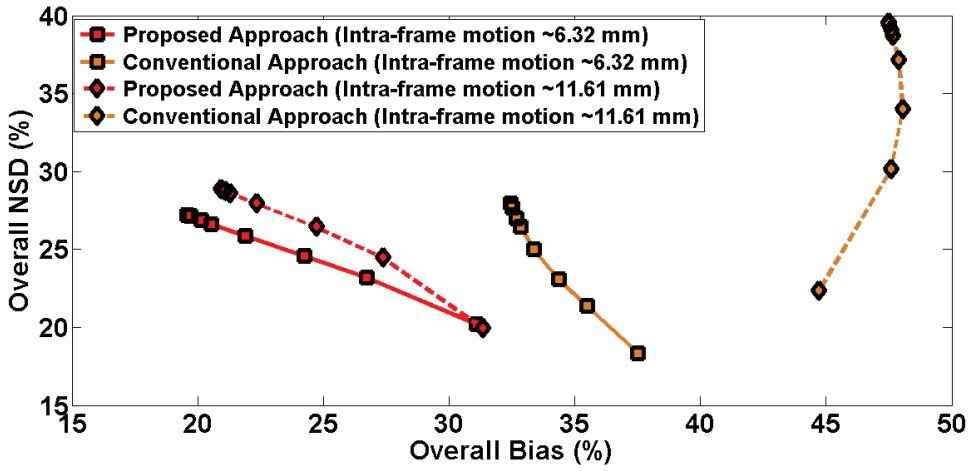

Figure 9. Overall noise-bias plots across deconvolution iterations 1, 2, 3, 5, 8, 10, 15, 20 respectively for 8 ROIs. Proposed approach shows a better noise-bias performance over conventional approach with a greater reduction in bias at a cost of smaller increase in noise levels.

5. Discussion

In the context of multi-frame PET images, incorporating the proposed transmission-emission alignment strategy, qualitative and quantitative analysis from simulations showed that our approach of intra-frame motion compensation produced images with superior quality (Figure 6), improved accuracy (Figure 7), and enhanced noise-bias performance (Figure 9). Error norm increased with intra-frame motion (Figure 8), which was attributed to the significant transmission-emission mismatch artifacts. However, even for high intra-frame motion, the proposed methodology of transmission-emission alignment and intra-frame motion compensation resulted in considerably less error norm (discrepancy) compared to the conventional approach and inter-frame only motion compensated images.

We note that our intra-frame motion correction approach relies on an accurate tracking of patient motion over time. The Polaris Vicra optical tracking system is utilized by a number of users and has resulted in enhanced reconstructions for different algorithms [8, 17, 21, 32]. Nonetheless, the use of this device has the potential to suffer from drifts of the cap on which the retro-reflective spheres are mounted or of the scalp with respect to the skull (e.g. due to rubbing of head against the bed). Tracking solutions that seek to minimize such issues are clearly preferred, an example of which has been the promising use of structured light motion tracking of the face [35], which can be utilized in the context of our proposed methodology.

We also note that for increasingly greater movements (i.e. larger $\overline{Disp}$; not shown), which are considerably less common (e.g. see [36], Figure 1), mismatch artifacts, though visually and quantitatively reduced with respect to conventional methods, can still be very significant even when using the proposed framework. For such motion levels, an alternative approach, which is a topic of future investigation, is to subdivide the frames into smaller sub-frames such that the mean motion, gauged by $\overline{Disp}$, falls below 6 mm. This approach, however, can degrade signal-to-noise for a given frame, and ultimately, a task-based optimization of motion-threshold may need to be achieved for optimal trade-off between the ability to compensate for motion and noise levels in individual sub-frames.

We also wish to point out that our method of allocating weights w_i purely by duration can be refined to incorporate the effect of decay into consideration. Consider the following simplistic scenario of a constant distribution within a frame: if we imagine two kinds of movements in a given frame, both of equal extent and duration, then a greater weight must actually be assigned to the earlier movement, since more disintegrations occur then than later due to the radioactive decay of the tracer. In many studies, however, frame durations are quite smaller than the half-life of the radiotracer; however, this is not always the case, and it is best if the weights are modified accordingly.

Two major drawbacks of deconvolution are noise propagation and the appearance of Gibbs artifacts. General approaches to this problem include early stopping of the algorithm, and/or the use of regularization. We performed inter-iteration regularization [37] using a Gaussian filter (2 mm FWHM). This approach was quite effective and was included in the entire study. Further improvements in image qualities may be obtained via the use of edge-preserving filtering [38-41]; this merits additional focus and systematic assessment, which is a topic of future work. Noise amplification and Gibbs artifacts can also be limited by an early stopping of deconvolution. Figure 7 shows that the optimal number of deconvolution iterations is less than five. This allows early stopping and, thereby, implicitly controls noise amplification and Gibbs overshoots in motion compensated images. Another potential approach to the general problem of Gibbs artifacts, which also appear in reconstruction-based resolution modeling [42] is to utilize specific post-reconstruction filters that suppress mid-frequencies [43]. Individual and or combined use of these methods remain to be systematically assessed for motion de-blurring.

Finally, we note that it is possible to explore the inclusion of motion-compensated iterative recovery within the EM reconstruction. An example has been to model motion blurring within the system matrix of the reconstruction algorithm [44], or to utilize optimization transfer to arrive at a nested framework for iterative, coupled image reconstruction and motion deblurring [45], as has also been explored in the context of resolution modeling [46]. It remains to be thoroughly evaluated in future work how these methods compare to one another.

We have demonstrated that reconstructing emission images with time-weighted average of motion transformed transmission images greatly reduces transmission-emission mismatches. Furthermore, coupled with a Richardson-Lucy deconvolution procedure to compensate for intra-frame motion, our proposed approach produces motion compensated images with superior quality compared to the conventional approach which is prone to noticeable transmission-emission mismatch artifacts.

Acknowledgments

The authors would like to thank Andrew Crabb for computation support, Nivedita Raghunath (GeorgiaTech) for helpful discussions and the reviewers for constructive comments. This work was supported by NIH grants MH078175 and 1S10RR023623.

References

1- R. N. Gunn, S. R. Gunn, F. E. Turkheimer, J. A. D. Aston, and T. J. Cunningham, "Positron Emission Tomography Compartmental Models: A Basis Pursuit Strategy for Kinetic Modeling," *Journal of Cerebral Blood Flow and Metabolism,* vol. 22, pp. 1425-1439, Dec 2002.

2- A. Rahmim and H. Zaidi, "Pet Versus Spect: Strengths, Limitations and Challenges," *Nucl Med Commun,* vol. 29, pp. 193-207, Mar 2008.

3- H. Zaidi and M. L. Montandon, "The New Challenges of Brain Pet Imaging Technology," *Current Medical Imaging Reviews,* vol. 2, pp. 3-13, 2006.

4- U. E. Ruttimann, P. J. Andreason, and D. Rio, "Head Motion During Positron Emission Tomography: Is It Significant?," *Psychiatry Res,* vol. 61, pp. 43-51, May 31 1995.

5- M. V. Green, J. Seidel, S. D. Stein, T. E. Tedder, K. M. Kempner, C. Kertzman*, et al.*, "Head Movement in Normal Subjects During Simulated Pet Brain Imaging with and without Head Restraint," *Journal of Nuclear Medicine,* vol. 35, pp. 1538-1546, Sep 1994.

6- P. M. Bloomfield, T. J. Spinks, J. Reed, L. Schnorr, A. M. Westrip, L. Livieratos*, et al.*, "The Design and Implementation of a Motion Correction Scheme for Neurological Pet.," *Phys Med Biol,* vol. 48, pp. 959-978, Apr 2003.

7- D. F. Wong, J. R. Brašić, H. S. Singer, D. J. Schretlen, H. Kuwabara, Y. Zhou*, et al.*, "Mechanisms of Dopaminergic and Serotonergic Neurotransmission in Tourette Syndrome: Clues from an in Vivo Neurochemistry Study with Pet," *Neuropsychopharmacology,* vol. 33, pp. 1239-1251, 2007.

8- B. J. Lopresti, A. Russo, W. F. Jones, T. Fisher, D. G. Crouch, D. E. Altenburger*, et al.*, "Implementation and Performance of an Optical Motion Tracking System for High Resolution Brain Pet Imaging.," *IEEE Trans Nuc Sci,* vol. 46, pp. 2059-2067, 1999.

9- L. Tellmann, R. Fulton, U. Pietrzyk, I. Nickel, I. Stangier, O. Winz*, et al.*, "Concepts of Registration and Correction of Head Motion in Positron Emission Tomography.," *Z Med Phys,* vol. 16, pp. 67-74, 2006.

10- O. A. van den Heuvel, R. Boellaard, D. J. Veltman, C. Mesina, and A. A. Lammertsma, "Attenuation Correction of Pet Activation Studies in the Presence

of Task-Related Motion.," *Neuroimage,* vol. 19, pp. 1501-1509, Aug 2003.

11- H. Herzog, L. Tellmann, R. Fulton, S. I, E. R. Kops, K. Bente*, et al.*, "Motion Artifact Reduction on Parametric Pet Images of Neuroreceptor Binding," *Journal of Nuclear Medicine,* vol. 46, pp. 1059-1065, Jun 2005.

12- N. Costes, A. Dagher, K. Larcher, A. C. Evans, D. L. Collins, and A. Reilhac, "Motion Correction of Multi-Frame Pet Data in Neuroreceptor Mapping: Simulation Based Validation," *Neuroimage,* vol. 47, pp. 1496-1505, Oct 1 2009.

13- R. R. Fulton, S. R. Meikle, S. Eberl, J. Pfeiffer, and C. J. Constable, "Correction for Head Movements in Positron Emission Tomography Using an Optical Motion-Tracking System.," *IEEE Trans Nuc Sci,* vol. 49, pp. 116-123, 2002.

14- A. Rahmim, O. G. Rousset, and H. Zaidi, "Strategies for Motion Tracking and Correction in Pet.," *PET Clinics,* vol. 2, pp. 251-266, 2007.

15- M. Daube-Witherspoon, Y. Yan, M. Green, R. Carson, K. Kempner, and P. Herscovitch, "Correction for Motion Distortion in Pet by Dynamic Monitoring of Patient Position (Abstract)." *J Nucl Med,* vol. 31, p. 816, 1990.

16- J. Qi and R. H. Huesman, "List Mode Reconstruction for Pet with Motion Compensation: A Simulation Study," *presented at the Proceedings IEEE International Symposium on Biomedical Imaging*, 7-10 July 2002, Washington, DC, USA, 2002.

17- R. E. Carson, W. C. Barker, J.-S. Liow, and C. A. Johnson, "Design of a Motion-Compensation Osem List-Mode Algorithm for Resolution-Recovery Reconstruction for the Hrrt," *presented at the IEEE Nuclear Science Symposium Conference Record, Portland, OR*, 2003.

18- A. Rahmim, P. Bloomfield, S. Houle, M. Lenox, C. Michel, K. R. Buckley*, et al.*, "Motion Compensation in Histogram-Mode and List-Mode Em Reconstructions: Beyond the Event-Driven Approach.," *IEEE Trans Nucl Sci,* vol. 51, pp. 2588-2596, Sep 21 2004.

19- P. Buhler, U. Just, E. Will, J. Kotzerke, and J. van den Hoff, "An Accurate Method for Correction of Head Movement in Pet.," *IEEE Trans Med Imaging,* vol. 23, pp. 1176-1185, Sep 2004.

20- C. Chan, X. Jin, E. K. Fung, M. Naganawa, T. Mulnix, R. E. Carson*, et al.*, "Event-by-Event Respiratory Motion Correction for Pet with 3d Internal-1d External Motion Correlation," *Medical physics,* vol. 40, p. 112507, 2013.

21- K. Dinelle, H. Ngo, S. Blinder, N. Vafai, G. Topping, and V. Sossi, "Frame-to-Frame Image Realignment Assessment Tool for Dynamic Brain Positron Emission Tomography," *Medical Physics,* vol. 38, pp. 773-781, Feb 2011.

22- S. H. Keller, M. Sibomana, O. V. Olesen, C. Svarer, S. Holm, F. L. Andersen*, et al.*, "Methods for Motion Correction Evaluation Using 18f-Fdg Human Brain Scans on a High-Resolution Pet Scanner," *J Nucl Med,* vol. 53, pp. 495-504, Mar 2012.

23- A. J. Montgomery, K. Thielemans, M. A. Mehta, F. Turkheimer, S. Mustafovic, and P. M. Grasby, "Correction of Head Movement on Pet Studies: Comparison of Methods.," *J Nucl Med,* vol. 47, pp. 1936-1944, Dec 2006.

24- T. L. Faber, N. Raghunath, D. Tudorascu, and J. R. Votaw, "Motion Correction of Pet Brain Images through Deconvolution: I. Theoretical Development and Analysis in Software Simulations," *Physics in Medicine and Biology,* vol. 54, pp. 797-811, Feb 7 2009.

25- N. Raghunath, T. L. Faber, S. Suryanarayanan, and J. R. Votaw, "Motion Correction of Pet Brain Images through Deconvolution: Ii. Practical Implementation and Algorithm Optimization," *Physics in Medicine and Biology,* vol. 54, pp. 813-829, Feb 7 2009.

26- H. Mohy-ud-Din, N. Karakatsanis, C. J. Endres, M. R. Ay, D. F. Wong, and A. Rahmim, "Generalized Inter-Frame and Intra-Frame Motion Correction in Dynamic Pet Imaging," *IEEE Nucl. Sci. Symp. Conf. Record,* vol. , pp. 3858-3862, 2011.

27- H. Mohy-ud-Din, N. A. Karakatsanis, J. S. Goddard, J. Baba, W. Willis, A. K. Tahari*, et al.*, "Generalized Dynamic Pet Inter-Frame and Intra-Frame Motion Correction: Phantom and Human Validation Studies," *Proc. IEEE Nucl. Sci. Symp. Conf.,* vol. , pp. 3067-3078, 2012.

28- W. H. Richardson, "Bayesian-Based Iterative Method of Image Restoration," *Journal of the Optical Society of America,* vol. 62, pp. 55-59, 1972.

29- L. B. Lucy, "An Iterative Technique for the Rectification of Observed Distributions," *Astronomical Journal,* vol. 79, pp. 745-754, 1974.

30- V. Sossi, H. W. A. M. de Jong, W. C. Barker, P. Bloomfield, Z. Burbar, M. L. Camborde*, et al.*, "The Second Generation Hrrt - a Multi-Centre Scanner Performance Investigation," in *Nuclear Science Symposium Conference Record, 2005 IEEE*, 2005, pp. 2195-2199.

31- A. Rahmim, K. Dinelle, J. C. Cheng, M. A. Shilov, W. P. Segars, S. C. Lidstone*, et al.*, "Accurate Event-Driven Motion Compensation in High-Resolution Pet Incorporating Scattered and Random Events,"

IEEE Trans Med Imaging, vol. 27, pp. 1018-33, Aug 2008.

32- K. Dinelle, S. Blinder, J. C. Cheng, S. Lidstone, K. Buckley, T. J. Ruth*, et al.*, "Investigation of Subject Motion Encountered During a Typical Positron Emission Tomography Scan," *2006 Ieee Nuclear Science Symposium Conference Record, Vol 1-6,* pp. 3283-3287, 2006.

33- B. K. Horn, "Closed-Form Solution of Absolute Orientation Using Unit Quaternions," *JOSA A,* vol. 4, pp. 629-642, 1987.

34- M. G. Ullisch, J. J. Scheins, C. Weirich, E. R. Kops, A. Celik, L. Tellmann*, et al.*, "Mr-Based Pet Motion Correction Procedure for Simultaneous Mr-Pet Neuroimaging of Human Brain," *Plos One,* vol. 7, Nov 12 2012.

35- O. V. Olesen, R. R. Paulsen, L. Hojgaard, B. Roed, and R. Larsen, "Motion Tracking for Medical Imaging: A Nonvisible Structured Light Tracking Approach," *Ieee Transactions on Medical Imaging,* vol. 31, pp. 79-87, Jan 2012.

36- X. Jin, T. Mulnix, J.-D. Gallezot, and R. E. Carson, "Evaluation of Motion Correction Methods in Human Brain Pet Imaging—a Simulation Study Based on Human Motion Data," *Medical physics,* vol. 40, p. 102503, 2013.

37- S. Mustafovic and K. Thielemans, "Object Dependency of Resolution in Reconstruction Algorithms with Interiteration Filtering Applied to Pet Data," *IEEE Transactions on Medical Imaging,* vol. 23, pp. 433-446, Apr 2004.

38- X. Geets, J. A. Lee, A. Bol, M. Lonneux, and V. Grégoire, "A Gradient-Based Method for Segmenting Fdg-Pet Images: Methodology and Validation," *European journal of nuclear medicine and molecular imaging,* vol. 34, pp. 1427-1438, 2007.

39- F. Hofheinz, J. Langner, B. Beuthien-Baumann, L. Oehme, J. Steinbach, J. Kotzerke*, et al.*, "Suitability of Bilateral Filtering for Edge-Preserving Noise Reduction in Pet," *EJNMMI research,* vol. 1, pp. 1-9, 2011.

40- G. Wang and J. Qi, "Penalized Likelihood Pet Image Reconstruction Using Patch-Based Edge-Preserving Regularization," *Medical Imaging, IEEE Transactions on,* vol. 31, pp. 2194-2204, 2012.

41- D. F. Yu and J. A. Fessler, "Edge-Preserving Tomographic Reconstruction with Nonlocal Regularization," *Medical Imaging, IEEE Transactions on,* vol. 21, pp. 159-173, 2002.

42- A. Rahmim, J. Qi, and V. Sossi, "Resolution Modeling in Pet Imaging: Theory, Practice, Benefits and Pitfalls," *Med Phys,* vol. 40, pp. 064301, 2013.

43- S. Tong, A. M. Alessio, K. Thielemans, C. Stearns, S. Ross, and P. E. Kinahan, "Properties and Mitigation of Edge Artifacts in Psf-Based Pet Reconstruction," *Nuclear Science, IEEE Transactions on,* vol. 58, pp. 2264-2275, 2011.

44- A. Rahmim, J. C. Cheng, K. Dinelle, M. Shilov, W. P. Segars, O. G. Rousset*, et al.*, "System Matrix Modelling of Externally Tracked Motion," *Nucl Med Commun,* vol. 29, pp. 574-81, Jun 2008.

45- N. A. Karakatsanis, H. Zaidi, and C. Tsoumpas, "Generalized 3d and 4d Motion Compensated Whole-Body Pet Image Reconstruction Employing Nested Em Deconvolution," in *Imaging Systems and Techniques (IST), 2014 IEEE International Conference on*, 2014, pp. 263-268.

46- G. I. Angelis, A. Reader, P. J. Markiewicz, F. A. Kotasidis, W. R. Lionheart, and J. Matthews, "Acceleration of Image-Based Resolution Modelling Reconstruction Using an Expectation Maximization Nested Algorithm," *Physics in medicine and biology,* vol. 58, p. 5061, 2013.